Gleeble-Assisted Investigation and Thermokinetics Simulation of α Phase Isothermal Precipitation during Short-Time Duplex Heat Treatment of Ti-6Al-4V Alloy

Nabil Kherrouba, Denis Carron, Ramdhane Kouba, Mabrouk Bouabdallah, Riad Badji

▶ **To cite this version:**

Nabil Kherrouba, Denis Carron, Ramdhane Kouba, Mabrouk Bouabdallah, Riad Badji. Gleeble-Assisted Investigation and Thermokinetics Simulation of α Phase Isothermal Precipitation during Short-Time Duplex Heat Treatment of Ti-6Al-4V Alloy. Journal of Materials Engineering and Performance, 2022, 31 (9), pp.7517-7526. ⟨10.1007/s11665-022-06775-8⟩. ⟨hal-04424452⟩

HAL Id: hal-04424452

https://hal.science/hal-04424452v1

Submitted on 28 Feb 2025

HAL is a multi-disciplinary open access archive for the deposit and dissemination of scientific research documents, whether they are published or not. The documents may come from teaching and research institutions in France or abroad, or from public or private research centers.

L'archive ouverte pluridisciplinaire **HAL**, est destinée au dépôt et à la diffusion de documents scientifiques de niveau recherche, publiés ou non, émanant des établissements d'enseignement et de recherche français ou étrangers, des laboratoires publics ou privés.

HAL Authorization

Gleeble-Assisted Investigation and Thermokinetics Simulation of α Phase Isothermal Precipitation during Short-Time Duplex Heat Treatment of Ti-6Al-4V Alloy

Nabil Kherrouba, Denis Carron, Ramdhane Kouba, Mabrouk Bouabdallah, and Riad Badji

The precipitation mechanism and kinetics of the secondary a phase during short-time duplex heat treat-ment of the Ti-6Al-4V alloy were investigated. The precipitation kinetics was determined by means of in situ isothermal electrical resistivity tests in a Gleeble thermomechanical testing machine in the temperature range of 600-700 □C. The results showed that the higher the aging temperature, the faster the secondary a phase precipitation, which obeys the Kolmogorov–Johnson–Mehl–Avrami (KJMA) equation with an Av-rami parameter n = 1. The precipitation process was also investigated by simulation using the thermoki-netic software MatCalc. Results of the simulation on MatCalc indicated that the secondary a phase nucleation ended at an earlier stage of the precipitation and that the latter is mainly controlled by the growth of secondary a phase precipitates. Increasing the aging temperature resulted in an increase of the precipitate□s size with an activation energy of Q = 62 kJ/mol for the process. Evolution of the simulated elements contents showed that only the vanadium concentration in the b phase changed significantly during the isothermal aging. Thus, the growth of the secondary a phase is governed by the vanadium diffusion into the b phase.

Keywords electrical resistivity, Gleeble, MatCalc, precipitation, simulation, Ti-6Al-4V

1. Introduction

Titanium alloys are widely used in industry due to their outstanding properties, particularly low density, good corrosion resistance and high mechanical properties (Ref 1-4). They undergo, during manufacturing, several thermomechanical treatments that generate a multitude of microstructures (Ref 5-7) and greatly affect the final mechanical properties of the alloy (Ref 8). Among titanium alloys, the Ti-6Al-4V alloy is the most used in industry (Ref 9). It exhibits, at room temperature, a microstructure composed of α and β phases. All of the proportions, morphologies and chemical composition of these phases strongly affect the ductility (Ref 10), the creep resistance (Ref 11, 12), the strength (Ref 13) and the fatigue resistance (Ref 14) of the alloy.

Nabil Kherrouba and **Riad Badji**, Research Center in Industrial Technologies CRTI, P.O. BOX 64, 16014 Cheraga, Algiers, Algeria; **Denis Carron**, IRDL, UMR CNRS 6027, Univ. Bretagne Sud, 56100 Lorient, France; **Ramdhane Kouba**, Laboratoire de Technologie des Matériaux, Département SDM, Faculté de Génie Mécanique et Génie des Procédés, USTHB, BP 32 El-Alia, 16111 Algiers, Algeria; and **Mabrouk Bouabdallah**, LGSDS – Ecole Nationale Polytechnique, 10 Avenue Hassan Badi, 16200 El Harrach, Algiers, Algeria. Contact e-mail: nabil.kherrouba@yahoo.fr.

Annealing below the normal recrystallization temperature, which is approximately 800 °C (Ref 15), is one of the operations that characterizes the thermomechanical processing underwent by Ti-6Al-4V alloy during its manufacturing. During this stage, temperature and duration of the annealing determine the secondary α phase precipitation and its volume fraction. This phase is known to enhance the strength and fracture toughness (Ref 16). It is, therefore, interesting to study and understand the thermodynamics and kinetics of its precipitation. Several attempts have been made to discuss and model the formation mechanism of the secondary α platelets during cooling in titanium alloys. Sun et al (Ref 17) investigated the formation mechanism of α phase by means of SEM observations. They stated that the secondary α phase platelets nucleated from the α_{GB} layer due to interface instability. They, also, suggested that the nucleation rate of the α_{GB} layer determines the secondary α phase platelets thicknesses. Previously, Texeira et al (Ref 18) used a nucleation mechanism based on the sympathetic nucleation from the α_{GB} layer to model the formation of the secondary α phase during cooling in a deformed near β titanium alloy. Furthermore, Fujii (Ref 19) reported that the α_{GB} morphology growth arrested in an earlier stage and that the $\beta \rightarrow \alpha$ phase transformation is mainly controlled by the growth mechanism of the secondary α platelets.

Semiatin et al. (Ref 20) have highlighted the effects of temperature and cooling rate on the microstructural evolutions of heat-treated Ti-6Al-4V in the ($\alpha + \beta$) field. They suggested a diffusion-controlled model based on the Trivedi and Bosze model (Ref 21, 22) to predict the growth of primary and secondary α phase morphologies as a function of supersatura-

Accepted Manuscript

tion, diffusivity coefficients and cooling rate. They assumed that small cooling rates did not permit the precipitation of the secondary α phase. Meng et al. (Ref 23) attributed this phenomenon to low supersaturations generated during these cooling rates. Indeed, low cooling rates favor the growth of primary α phase, whereas high cooling rates generate high supersaturations, which are beneficial to the nucleation and growth of secondary α phase. Katzarov et al. (Ref 24) studied the secondary α phase formation during heat treatment in the β domain and developed a numerical simulation based on the nucleation-growth theory to describe the apparition of α-Widmanstatten plates. Malinov et al. (Ref 25) studied the isothermal $\beta \rightarrow \alpha$ phase transformation in the Ti-6Al-4V alloy in the framework of the Kolmogorov–Johnson–Mehl–Avrami (KJMA) equation. They used electrical resistivity to determine the kinetics parameters and stated that the $\beta \rightarrow \alpha$ phase transformation is characterized by the existence of two mechanisms of α phase formation whether the aging temperature is above or below 900 °C.

Besides, further researches have been conducted to expand the industrial application of the Ti-6Al-4V alloy by improving its strength. This was achieved by studying effects of short-time duplex heat treatment on the mechanical properties of the alloy (Ref 26-28). This heat treatment consists first on a solution annealing at temperature in the ($\alpha + \beta$) domain, followed by a second isothermal holding at lower temperature. Reda et al. (Ref 29) investigated effects of the single and duplex short-time heat treatments on the microstructure and mechanical properties of a Ti-6Al-4V alloy and stated that higher amounts of retained β phase obtained after duplex short heat treatment impacts greatly the alloy strengthening. Ajiz et al. (Ref 30) reported in their work that optimum values of yield strength and tensile strength were obtained after short-time solution treatment at 930 °C for 60 s, followed by isothermal aging at 530 °C for 40 s. Morita et al. (Ref 31) investigated the mechanical behavior of a Ti-6Al-4V alloy subjected to short-time solution annealing at 930 °C and 960 °C for 60 s and then quenched. They reported that these heat treatments engendered a rise in the tensile strength and the fatigue strength and attributed this improvement to the apparition of fine acicular α' martensite phase.

All these previous works reveal the great interest of studying the different microstructural evolutions issued from heat treatments and their effects on the final properties of the Ti-6Al-4V alloy. These microstructural evolutions depend mainly, as indicated in the above mentioned literature, on the heating/cooling rates, growth of primary α phase, nucleation and growth of secondary α phase but also on the isothermal holding stage in the ($\alpha + \beta$) domain. Nevertheless and at the authors' knowledge, there is a lack of documentation concerning kinetics accompanying short-time heat treatments. Accordingly, the aim of the present work is to propose a predictive simulation of thermodynamic and nucleation-growth kinetics of the secondary α phase precipitation in the Ti-Al-V system and discuss its nucleation-growth mechanisms during short-time solution annealing at 800 °C, followed by isothermal aging in the temperature range 600-700 °C for 300 s. Results of the simulation were compared to the experimental results issued from in situ electrical resistivity tests conducted on the Ti-6Al-4V two-phase titanium alloy in the ($\alpha + \beta$) domain by using a Gleeble 3500 thermomechanical testing machine.

2. Materials and Methods

The material studied in the present work was a Ti-6Al-4V titanium two-phase alloy whose chemical composition, determined using an Oxford Foundry Master Pro Optical Emission Spectrometer, is given in Table 1. The alloy was supplied in the form of 2-mm-thick sheets.

2.1 Thermodynamic and Thermokinetics Simulations

The thermodynamic and thermokinetics calculations were performed with the MatCalc software. To this purpose, thermodynamic and diffusion databases for the Ti-Al-V system were used. The thermodynamic calculations (at equilibrium) were carried out using the Gibbs energy minimization method, which allows to determine the stable phases at a given temperature and to plot the phase diagram of the alloy.

The phase transformations kinetics were simulated in MatCalc by using the nucleation-growth theory, in which the critical energy barrier for the formation of a stable nucleus is given by:

$$\Delta G^{*} = \frac{16\pi}{3}\frac{\gamma^{3}}{\Delta G_{\mathrm{vol}}^{2}} \quad \text{(Eq 1)}$$

where ΔG_{vol} is the volume free energy change for the formation of the nucleus, γ is the interfacial energy and is given assuming the generalized-broken-bond model (Ref 32). The precipitate's growth is described by using the Svoboda-Fischer-Fratzl-Kozeschnik (SFFK) growth model (Ref 33). The formalism of the MatCalc model is based on the thermodynamic extremal principle, which states that during the growth of the precipitates, the system evolves by dissipating the maximum of its entropy (Ref 32). Performing the precipitation setup using MatCalc requires to define a precipitation domain (which is the β matrix phase in the present work) and α as the precipitated phase. Heterogeneous germination is taken into account by considering that the germination sites are the dislocations in the β matrix. The plate-like shape of the precipitates is included in the simulation setup by introducing a shape factor with a value of 0.1. MatCalc simulation permits to predict the precipitation kinetics and thus to follow the evolution of all aspects of the process as a function of time. In the present work, the focus will be on the evolution of the fraction of precipitates, their size and density, as well as nucleation rate and chemical composition of precipitates and matrix.

2.2 Electrical Resistivity

The electrical resistivity is one of the most sensitive techniques used to study phase transformations particularly those occurring in titanium alloys (Ref 34-36). In the present work, in situ electrical resistivity tests were conducted in a Gleeble 3500 machine to determine normalized fraction of the secondary α phase that precipitated from the supersaturated β

Table 1 Chemical composition of the Ti-6Al-4V alloy

Element	Ti	Al	V	Fe	O	C	N
wt.%	Balance	6.24	3.83	0.20	0.18	0.01	0.01

Accepted Manuscript

phase in the ($\alpha + \beta$) domain. The Gleeble 3500 is a fully integrated digital closed-loop control thermal and mechanical testing system. It includes a high-speed heating system, a servo hydraulic system and a computer control and data acquisition system. In this study, $120\times5\times2$ mm^3 bars were machined to perform the tests. The bars were mounted between two stainless steels "hot" grips in the Gleeble chamber. Three K-type thermocouples TC_1, TC_2 and TC_3 were spot-welded on the surface of each specimen. TC_1 was at mid-length, TC_2 and TC_3 were at $\pm$ 5 mm from TC_1. Two wires of pure platinum were also welded on the surface diametrically opposed to TC_2 and TC_3 as indicated in Figure 1(a). The pure platinum's wires were used to measure the voltage during the in situ electrical resistivity test. The heat treatment that the sample underwent was monitored by the TC_1 thermocouple welded in the center of the sample. The "hot" grips used in the present experiments guaranteed a low axial thermal gradient during the test and ensured that the temperature in the area defined by the thermocouples TC_2 and TC_3 remained almost constant. The heat treatment is an "interrupted quenching," i.e., a stepped quenching, where the sample is cooled very fast from 800 °C to the desired temperature (600, 650 and 700 °C), kept at this temperature and finally quenched to room temperature. The bars were heated up under secondary vacuum to 800 °C, i.e., annealed in the $\alpha + \beta$ field, at a heating rate of 10 °C/min; they were then soaked at this temperature for 5 min and rapidly cooled to the desired temperatures (600, 650 and 700 °C). At last, they were isothermally held at these temperatures for five minutes in which electrical resistivity was measured. A nozzle was used to blow helium inert gas on the sample to enhance the cooling rate during the interrupted quench (Figure 1b). For instance, the cooling rate from 800 to 700 °C was about 370 °C.s^{-1} (Figure 6).

3. Results and Discussions

3.1 Microstructural Evolution

Figure 2 shows the microstructure of the as-received alloy. It consists of a matrix of light colored α phase and intergranular dark colored β grains. An example of microstructures obtained after the short-time heat treatment on the Gleeble machine is depicted in Figure 3. The isothermal holding at 600 °C during 5 min induced an increase in the β grain size from approximately 3.4 $\pm$ 0.9 μm for the as-received sample to 8.7 $\pm$ 1.2 μm for the heat treated one. Besides, the microstructure obtained after the short-time heat treatment is composed of the untransformed primary α phase and a mixture of precipitated secondary α phase platelets and residual β phase.

3.2 Thermodynamic Calculations

Figure 4 shows the pseudo-binary phase diagram of the Ti-Al-V system at 90 wt.% Ti as obtained from the MatCalc software. The dashed line indicates the composition of the Ti-6Al-4V alloy. It is noticed from this diagram that the beta-transus temperature T_β is approximately 970 °C, which is 25 °C below the T_β previously estimated by differential scanning calorimetry (DSC) (Ref 37). This difference is probably due to the effect of the chemical composition as reported in the literature (Ref 3). Indeed, in the simulation, the system Ti-Al-V (with only Ti, Al and V elements) was considered, whereas in the DSC test, the alloy with the chemical composition given in Table 1 was used. In addition, thermodynamic calculations predicted the existence of the Ti_3Al intermetallic compound at low temperatures. In a previous work (Ref 38), the authors have investigated the microstructural evolutions of the same alloy and have not noticed the presence of this phase. Elmer et al. (Ref 39), who used the Thermo-Calc software to determine the phase equilibria of the Ti-6Al-4V alloy, have also reported similar results and noticed the absence of the Ti_3Al compound. Besides, Lutjering (Ref 3) stated that the Al content is generally limited to 6 wt.% in most titanium alloys to avoid the apparition of the Ti_3Al phase.

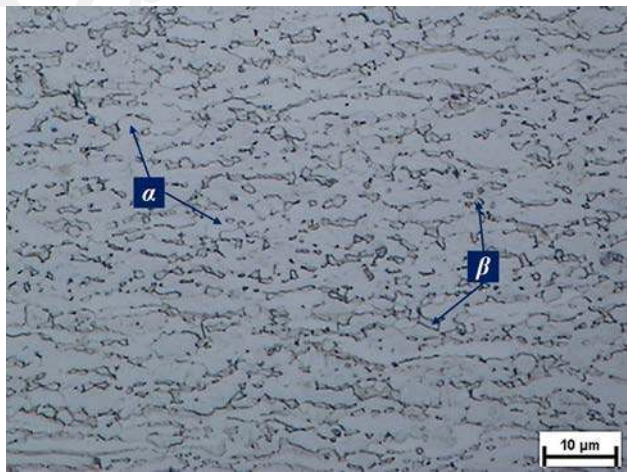

Fig. 2 As received alloy microstructure

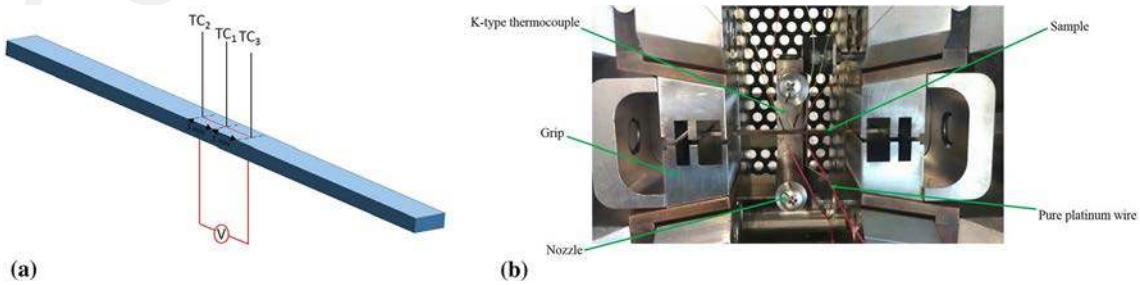

Fig. 1 (a) Schematic illustration of the Gleeble specimen with spot-welded thermocouples and platinum's wires for voltage measurement. (b): The Gleeble 3500 vacuum chamber with mounted specimen for in situ resistivity measurement

Accepted Manuscript

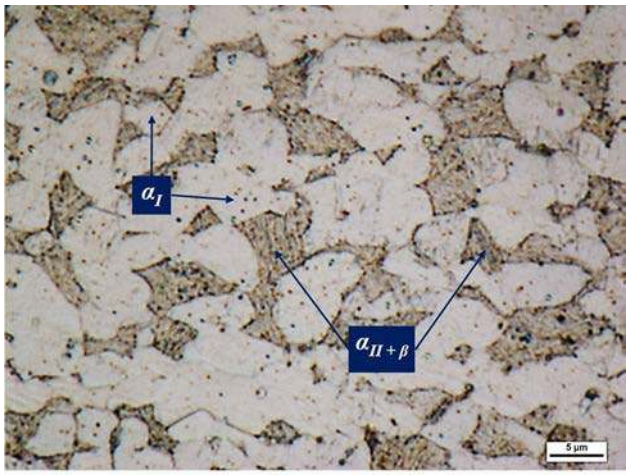

(a)

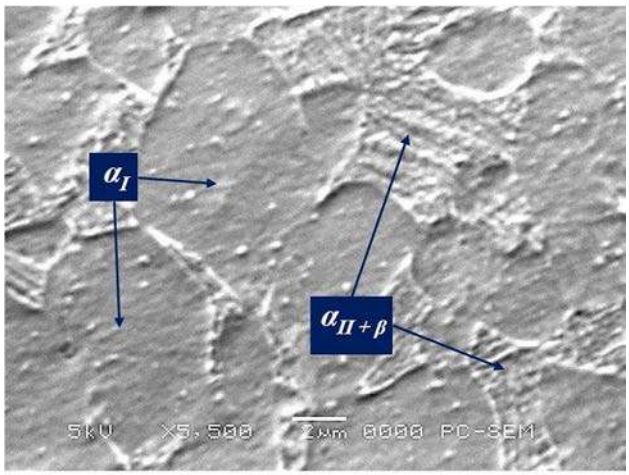

(b)

Fig. 3 Microstructure induced by the short-time heat treatment at 600 °C (a) optical micrographic, (b) SEM micrographic

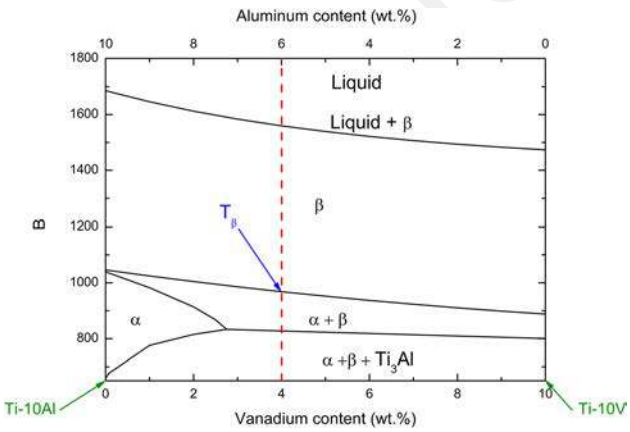

Fig. 4 Calculated pseudo-binary phase equilibrium diagram obtained by using MatCalc for the Ti-6Al-4V system at 90 wt.% Ti. The dashed line represents the nominal Ti-6Al-4V alloy composition

3.3 Experimental Kinetics of the Isothermal Precipitation of Secondary a Phase in the (a + b) Domain

Generally, the electrical resistivity evolution in a material depends on several factors such as precipitation phenomenon, matrix enrichment in solute and vacancies density (Ref 40). However, Burke (Ref 41) reported that the electrical resistivity is mainly dependent on the precipitation phenomenon when the test is made during isothermal heat treatment and that it is proportional to the transformed fraction. The electrical resistivity ρ was estimated, in the present work, by using the following formula:

$$R = \frac{\rho L}{S} \quad \text{(Eq 2)}$$

where R is the electrical resistance, L is the sample's length, and S is its cross section area.

Differentiating Eq 2 permitted to write:

$$\frac{\Delta R}{R} = \frac{\Delta \rho}{\rho} + \frac{\Delta L}{L} + \frac{\Delta S}{S} \quad \text{(Eq 3)}$$

It is reported in the literature (Ref 42, 43) that the $\beta \rightarrow \alpha$ phase transformation in titanium alloys is not accompanied with a significant volume change. Thus, equation 3 can be written as:

$$\frac{\Delta R}{R} = \frac{\Delta \rho}{\rho} \quad \text{(Eq 4)}$$

The evolution of the in situ relative electrical resistivity as a function of the time for the different aging temperatures is depicted in Fig. 5. The electrical resistivity curve exhibits a sigmoidal shape at each aging temperature. The relative electrical resistivity increases continuously during the isothermal holding and finally reaches its equilibrium value. It is also noticed from Fig. 5 that the electrical resistivity reached its equilibrium value earlier when the aging temperature is higher.

Semiatin et al. (Ref 20) reported that during heat treatment in the (α + β) domain, the secondary α phase platelets precipitated entirely within the β phase. Besides, they indicated that during these heat treatments, coarsening of primary α phase

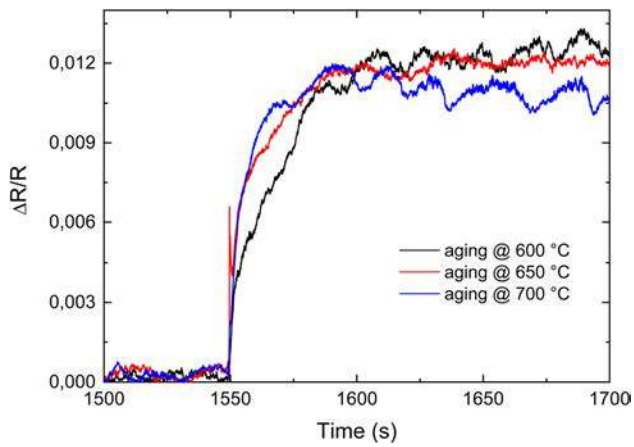

Fig. 5 Relative electrical resistivity variation $\Delta R/R = f(t)$ during isothermal aging of the Ti-6Al-4V alloy

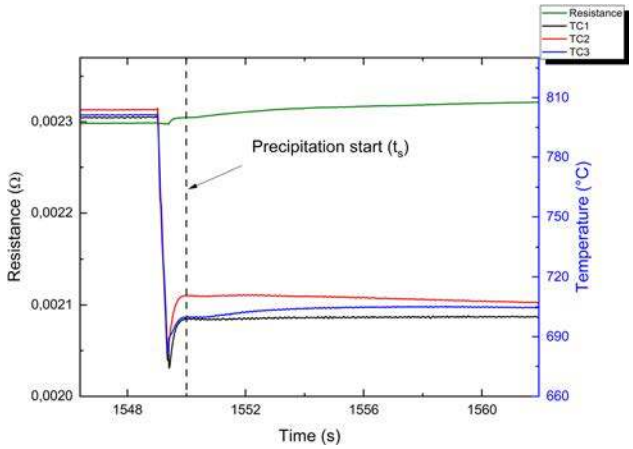

Fig. 6 Temperature undershoot at the beginning of the isothermal aging at 700 °C and determination the precipitation starting time t_s

requires a long time (about 64 h or more). Moreover, the solution annealing was achieved at temperature below the Ms temperature (Ref 37) to prevent the apparition of martensite. Thus, in the present study, only the decomposition of the supersaturated β phase is considered responsible of the secondary α phase precipitation. The $\beta \rightarrow \alpha$ phase transformation is known to be fast enough in titanium alloys (Ref 25); therefore, the in situ tests conducted in the present work were convenient to study the decomposition of the supersaturated β phase in the ($\alpha + \beta$) domain. However, it was crucial to accurately determine instants at which this transformation started and ended. Figure 6 indicates that the interrupted quench from 800 °C had induced an under-shoot before the temperature stabilized after few seconds. In order to determine the kinetics of the secondary α phase precipitation, this fluctuation should be eliminated. This was achieved by choosing the starting time t_s just after the under-shoot as indicated in Fig. 6 for aging at 700 °C. The time at which the phase transformation ended t_f was estimated from the derivative signal of the electrical resistivity. The instant t_f corresponds to the moment when this derivative is zero as indicated in Fig. 7(a) and (b).

Once t_s and t_f are determined, the normalized transformed fraction y is given by using the equation:

$$y = \frac{\rho(t,T) - \rho_s(T)}{\rho_f(T) - \rho_s(T)} \quad \text{(Eq 5)}$$

where ρ_s, ρ_f and ρ are the electrical resistivity measurements at t_s, t_f and t, respectively.

Consequently, the normalized transformed fraction y can be estimated by using the following expression:

$$y = \frac{R(t,T) - R_i(T)}{R_f(T) - R_i(T)} \quad \text{(Eq 6)}$$

Using equation (6), the experimental normalized transformed fraction was estimated and its evolution with aging time was plotted as shown in Fig. 8(a). The curves exhibit a typical sigmoidal shape, which indicates that the $\beta \rightarrow \alpha$ phase transformation obeys the KJMA model. This permits to express the normalized transformed fraction as follows:

$$y = 1 - \exp[-(kt)^n] \quad \text{(Eq 7)}$$

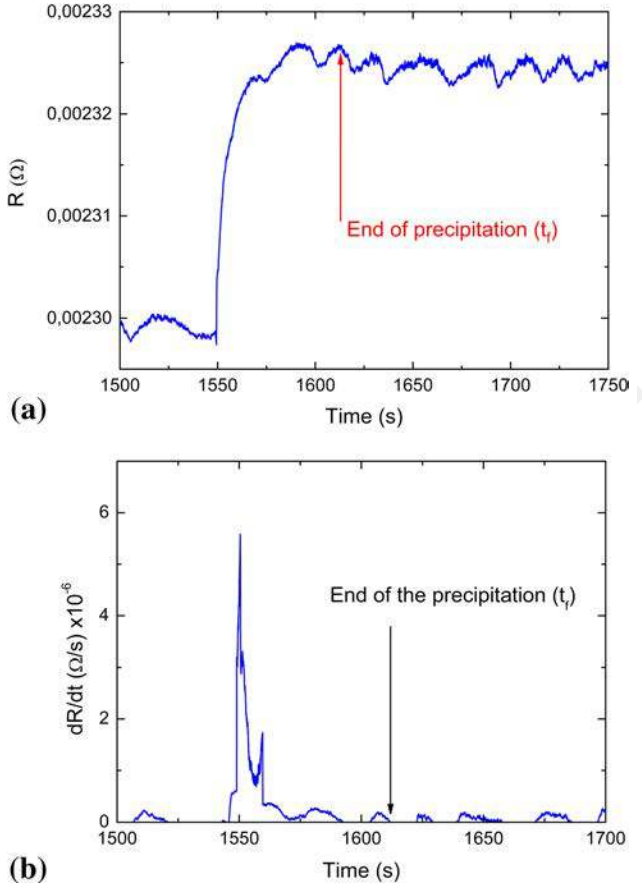

Fig. 7 Evolution at 700 °C of (a) the electrical resistivity signal $R = f(t)$ and (b) the electrical resistivity derivative signal dR/dt with determination of the precipitation ending time t_f

Thus, the plot of ln[ln (1/(1-y))] as a function of ln(t) was a straight line as illustrated in Figure 8(b). The Avrami index n and the rate constant k were determined from the slope and the intersection of the curve with the vertical axis, respectively. The different values of n and k obtained in the present work are given in Table 2. It is obviously noticed that an approximately unique value of $n = 1$ was obtained for all the applied temperatures. According to the classical nucleation-growth theory (Ref 44), a value of $n = 1$ may correspond to the thickening of platelets after site saturation. Bein and Béchet (Ref 36) reported that for a same value of $n = 1$, the nucleation occurred rapidly and the main parameter that governed the precipitation would be the diffusion-controlled growth of a fixed number of α platelets. Malinov et al. (Ref 25) argued that this value of $n = 1$ is attributed to grain boundary nucleation after saturation of α platelets for diffusion controlled growth.

A similar value of n calculated in the present work was already obtained in a previous work (Ref 45) where the $\beta \rightarrow \alpha$ phase transformation during cooling was studied. This is the consequence of using the same approach based on the KJMA equation in both continuous cooling and isothermal holding. Indeed, the continuous cooling was assimilated to a succession of isothermal steps where the KJMA equation was applied in each step. The additivity rule was, then, applied to adapt the KJMA equation to the non-isothermal conditions. However, some differences between the two conditions are noticed. In the non-isothermal heat treatment, the samples were cooled from

Accepted Manuscript

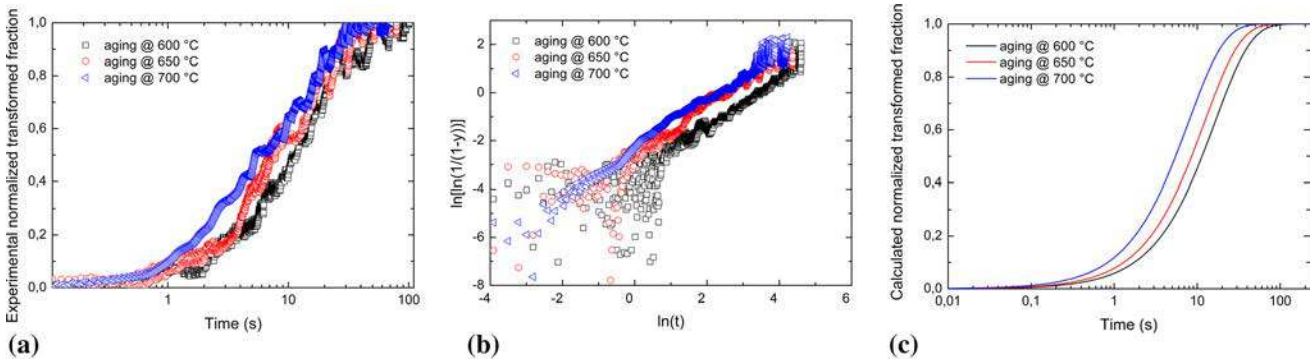

Fig. 8 Secondary α isothermal precipitation kinetics at 700 °C (a) experimental normalized transformed fraction, (b) application of the classical KJMA model , (c) calculated normalized transformed fraction

Table 2 Kinetic parameters of the KJMA equation

	600	650	700
n	1.01	0.98	0.99
k (s^{-1})	0.05	0.08	0.12

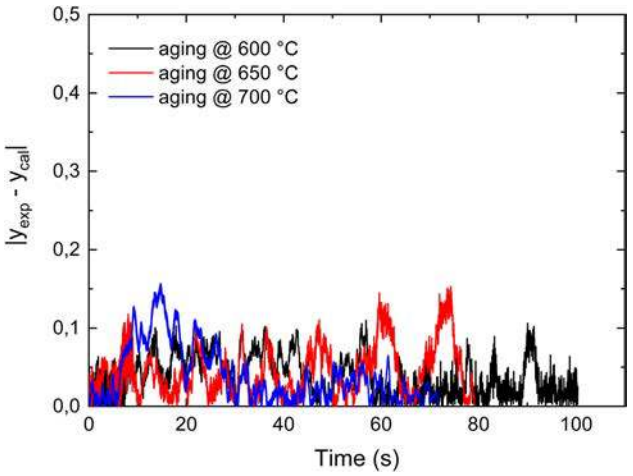

Fig. 9 Difference between experimental and calculated normalized transformed fractions $|y_{exp} - y_{cal}|$

the single β phase domain, whereas they were annealed in the (α + β) domain in the present work. Furthermore, during continuous cooling, the microstructural evolutions in each isothermal step resulted from the previous stages, and the undercooling was generally conditioned by the cooling rate, yet remained almost low. However, for the isothermal holding, the undercooling was high since the cooling from the annealing temperature happened rapidly. Nevertheless, finding the same value for the Avrami index is consistent with the secondary α phase morphology, which was observed in the literature. Figure 8(c) shows the calculated normalized transformed fractions (obtained using the KJMA equation) as a function of temperature with an Avrami index n = 1 for the specimens that were isothermally treated at different temperatures between 600 and 700 °C. The comparison between these normalized transformed fractions and those determined experimentally is depicted in Fig. 9, which shows a good agreement between

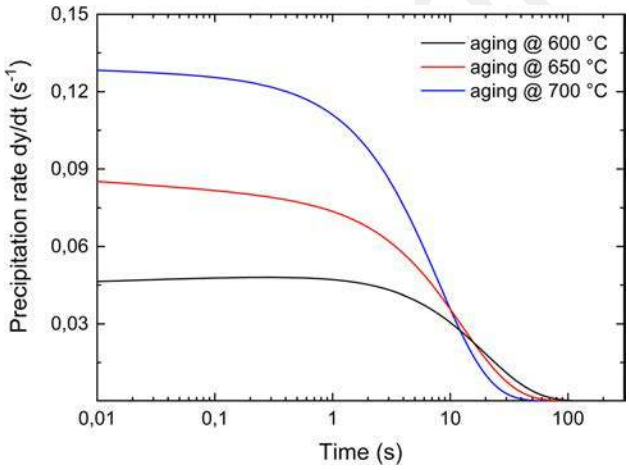

Fig. 10 Precipitation rate dy/dt vs aging time at 600, 650 and 700 °C.

them. It is noticed from Fig. 8(c) that the normalized transformed fraction curves shifted toward long aging times when the temperature becomes lower. This statement is clearly highlighted in Fig. 10 and Table 2, where the precipitation rate dy/dt and the k values are given, respectively. Indeed, k increased with the aging temperature, whereas the precipitation rate started at a higher value before to decrease rapidly when the aging temperature is higher. Thus, the fastest precipitation kinetics was obtained during aging at the highest temperature even though the undercooling was lower at this temperature. This could be explained by considering the competition between the undercooling—which is the driving force for nucleation of the secondary α phase—and diffusion of the β stabilizing elements, (particularly vanadium) that controls the secondary α phase growth. This will be thoroughly detailed in the simulation part of the present work. A comparison between values of the rate constant k obtained in this study and those reported by Malinov et al. (Ref 25) shows that the isothermal precipitation of secondary α phase was faster when the alloy underwent the short-time duplex heat treatment.

The overall activation energy of the secondary α phase precipitation has been calculated from the evolution of k with temperature assuming the following equation:

$$k = k_0 \exp\left(-\frac{Q}{RT}\right) \quad \text{(Eq 8)}$$

where k_0 is a pre-exponential constant and Q is the overall activation energy of the secondary α phase precipitation. It is noticed from Figure 11 that the $\ln(k) = f(1/T)$ curve exhibits a linear tendency. A simple linear regression allowed to determine the activation energy of the secondary α phase precipitation, Q = 62 kJ/mol with a coefficient of determination R_2 = 0.99.

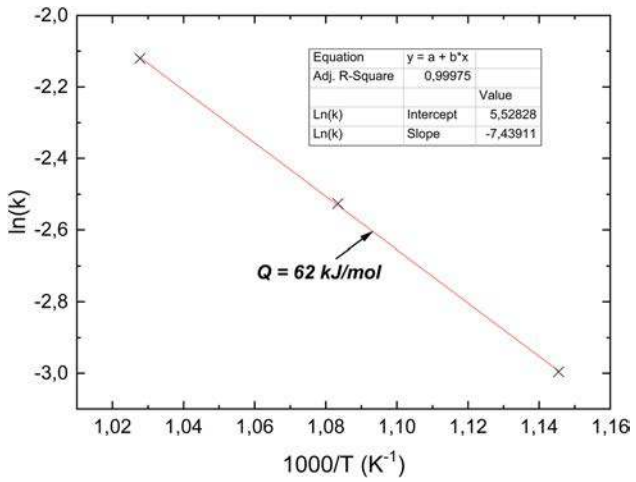

Fig. 11 Determination of the overall activation energy for the secondary α phase precipitation

3.4 Thermokinetic Precipitation Simulation Using MatCalc

Evolutions of the simulated and experimental transformed fractions with the aging time are depicted in Fig. 12, which shows a good agreement between the results issued from simulation with MatCalc and the experimental normalized transformed fractions with a satisfactory coefficient of determination R^2 = [0.96-0.98].

Figure 13 shows an example of evolutions of the nucleation rate and the number of precipitates during the isothermal aging at 600 °C. It is noticed from this figure that the nucleation rate reaches a maximum value of 8.2×10^{21} $m^{-3}.s^{-1}$ before it decreases and attains the zero value. Simultaneously, the number of precipitates increases rapidly and reaches 6×10^{20} m^{-3}. Once the nucleation sites are consumed, the precipitates' number remains constant. It is worth noticing that the nucleation stage was achieved after only 0.3 s. Therefore, it ended at the beginning of the β phase decomposition. Similarly, for all aging temperatures between 600 and 700°C, the secondary α phase nucleation ended at the beginning of the precipitation, which indicates that its precipitation is mainly controlled by the precipitate's growth. Effect of the aging temperature on the nucleation rate and the precipitates number is highlighted in Fig. 14 and 15, respectively. It can be seen that the maximum nucleation rate increased with the aging temper-

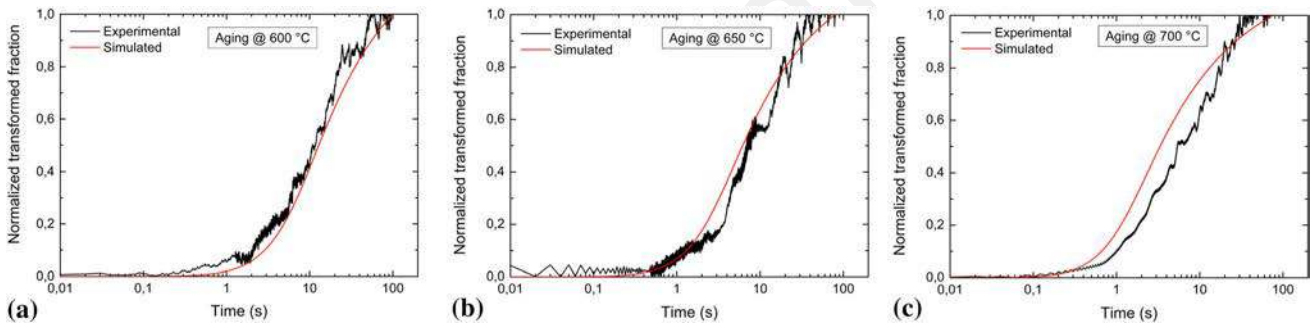

Fig. 12 Evolution of the experimental and MatCalc simulated normalized transformed fraction with aging time at (a) 600 °C, (b) 650 °C and (c) 700 °C

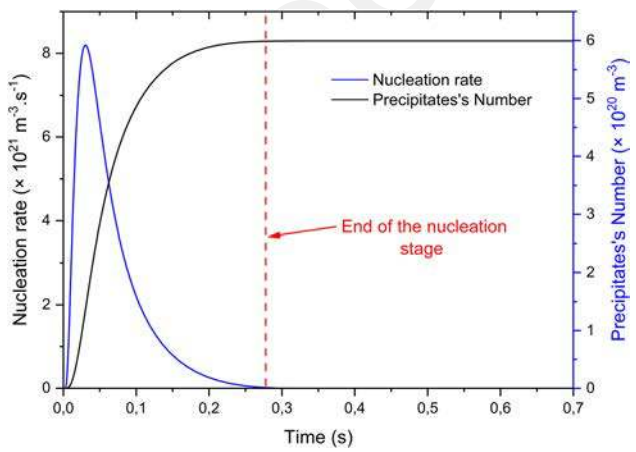

Fig. 13 Simulated nucleation rate and precipitates' number vs aging time at 600 °C

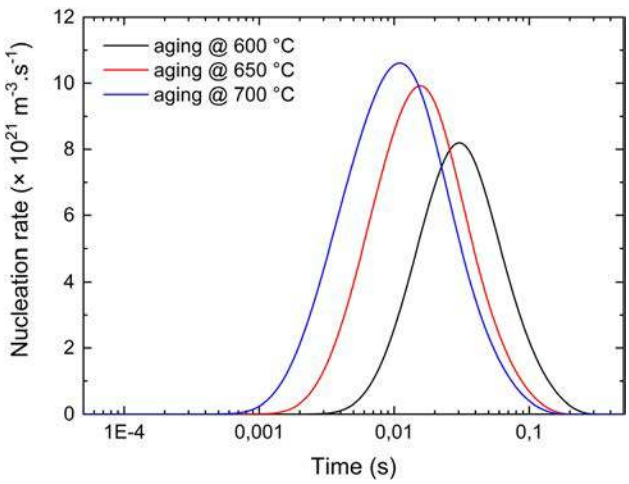

Fig. 14 Effect of the aging temperature on the simulated nucleation rate

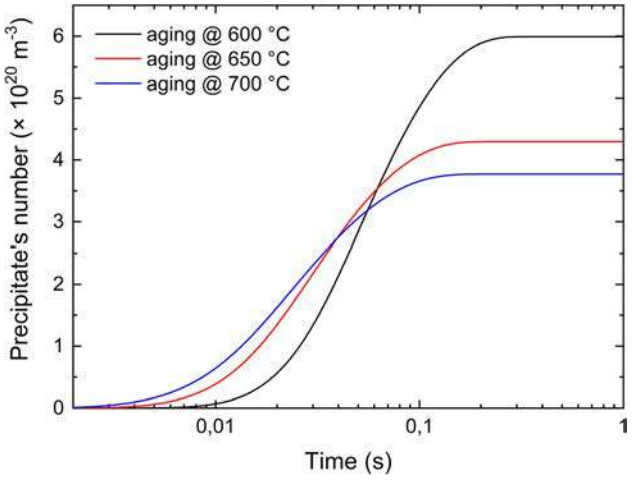

Fig. 15 Effect of the aging temperature on the simulated number of precipitates

ature. This can be explained by considering the effect of the solute content as reported by Porter and Easterling (Ref 46), who indicated that alloys with less solute content exhibited lower nucleation rate. Thus, as noticed from the pseudo-binary phase diagram of the Ti-Al-V system (Fig. 4), the solubility of vanadium in α phase decreased with temperature below 800 °C, which lowered the nucleation rate. Besides, increasing the aging temperature permitted to obtain secondary α phase with high precipitates size, which reduced the number of the secondary α phase particles.

An example of evolution of the aluminum and vanadium concentrations at 600 °C, in both α and β phases, with time is given in Fig. 16(a). It can be obviously noticed that only the vanadium content in the β phase changed significantly. Indeed, the aluminum content in both α and β phases and the vanadium content in the α phase were almost constant, whereas the vanadium content in the β phase increased from 15 to 32 wt.%.

Figure 16(b) shows that the vanadium content (reached at the end of the isothermal aging) in both α and β phases increases with the temperature. As mentioned above, the vanadium equilibrium concentration depends on the temperature and the solubility of vanadium in α phase raises with temperature. Accordingly, during their growth, the secondary α phase platelets, reject vanadium to the regions between them. The vanadium attains high amounts at these regions and strongly stabilizes the remaining β phase.

An example of the precipitate size distribution for the isothermal aging at 600 °C after solution annealing at 800 °C is illustrated in Fig. 17. The MatCalc software permitted to fit this distribution by using the Lifshitz–Slyozov–Wagner (LSW) distribution, which is one of the developed theories to model the diffusion-controlled coarsening of second-phase particles (Ref 47). Result of the fit is given in Fig. 17 with a coefficient of determination $R^2 = 0.85$. Thus, the insight of the possibility to obtain a coarsened microstructure during isothermal aging in the ($\alpha + \beta$) domain needs to be further investigated and documented even though several studies have been dedicated to

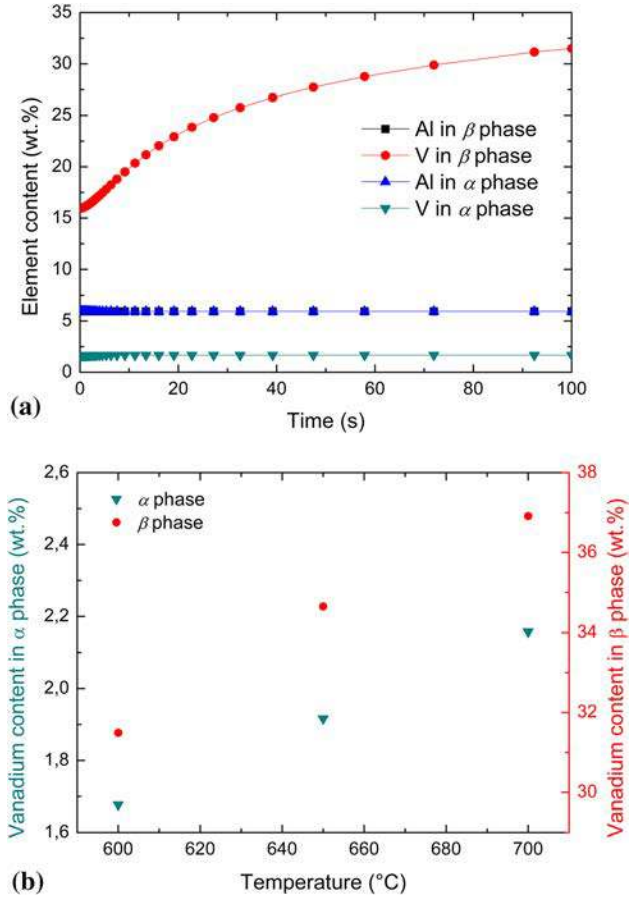

Fig. 16 Chemical composition in both α and β phases: (a) change of aluminum and vanadium concentrations during isothermal aging at 600 °C, (b) equilibrium vanadium content for the different aging temperatures

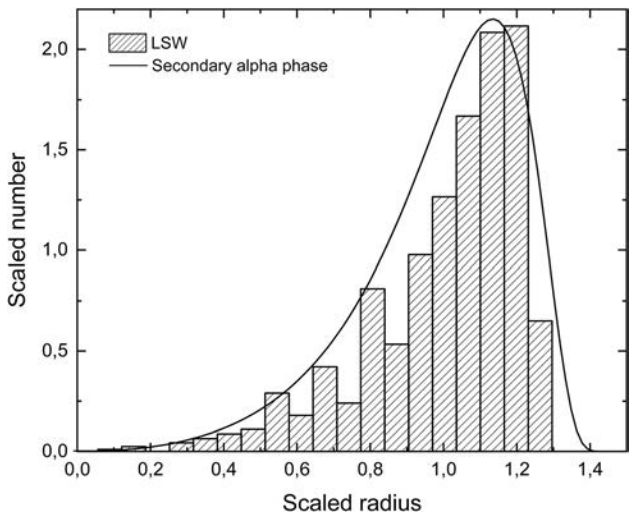

Fig. 17 Comparison between the precipitate size distribution as obtained by MatCalc and the Lifshitz-Slyozov-Wagner (LSW) distribution model

the coarsening mechanism in the hot-worked Ti-6Al-4V alloy (Ref 48-50).

4. Conclusions

The secondary α phase precipitation kinetics during short-time duplex heat treatment at different temperatures into the (α + β) domain in the Ti-6Al-4V alloy has been investigated. The main findings are drown as follows:

- Precipitation kinetics were conveniently determined by in situ electrical resistivity with the Gleeble 3500 testing machine
- Exploitation of results using classical KJMA model and microstructural observations permitted to determine all the kinetics parameters and discuss the microstructural evolutions of the secondary α phase precipitation.
- Simulation on MatCalc allowed to fully investigate the nucleation-growth mechanisms of the precipitation particularly evolutions of the nucleation rate, the precipitate's number and elements contents.
- All these findings suggest that the secondary α phase precipitation is mainly controlled by the growth of secondary α precipitates, which in turn is governed by the vanadium diffusion into the β phase.

Acknowledgments

This work was supported by a Doctorate fund of the Ministry of Higher Education and Scientific Research of Algeria and was a part of a research project at the Research Center in Industrial Technologies (CRTI). Dr. E. Povoden-Karadeniz (Vienna University of Technology) is gratefully acknowledged for graciously making available the thermodynamic and diffusion databases of the Ti-Al-V system for the MatCalc simulation. The Gleeble 3500 machine of Université de Bretagne-Sud was co-funded by the European Regional Development Fund. The authors would like to thank Mr. W. Berckmans (Univ. Bretagne-Sud) for the efforts he has put into completing the Gleeble tests.

References

1. S. Banerjee and P. Mukhopadhyay, *Phase Transformations: Examples from Titanium and Zirconium Alloys*, Elsevier, Amsterdam, 2010
2. M.J. Donachie, Titanium: A Technical Guide, 2nd ed., (ASM International, 2000)
3. G. Lütjering and J.C. Williams, *Titanium*, Springer Science & Business Media, Berlin, 2007
4. C. Leyens and M. Peters Eds., *Titanium and Titanium Alloys*, Wiley-vch, Amsterdam, 2003
5. T. Ahmed and H.J. Rack, Phase Transformations During Cooling in α + β titanium alloys, *Mater. Sci. Eng. A*, 1998, **243**, p 206–211. https://doi.org/10.1016/s0921-5093(97)00802-2
6. F.J. Gil, M.P. Ginebra, J.M. Manero, and J.A. Planell, Formation of α-Widmanstätten Structure: Effects of Grain Size and Cooling Rate on the Widmanstätten Morphologies and on the Mechanical Properties in Ti6Al4V Alloy, *J. Alloys Compd.*, 2001, **329**, p 142–152. https://doi.org/10.1016/S0925-8388(01)01571-7
7. K. Abbasi, B. Beidokhti and S.A. Sajjadi, Microstructure and Mechanical Properties of Ti-6Al-4V Welds using α, Near-α and α+β Filler Alloys, *Mater. Sci. Eng. A*, 2017, **702**, p 272–278. https://doi.org/10.1016/j.msea.2017.07.027
8. J. Sieniawski, R. Filip, and W. Ziaja, The Effect of Microstructure on the Mechanical Properties of Two-Phase Titanium Alloys, *Mater. Des.*, 1997, **18**, p 361–363. https://doi.org/10.1016/S0261-3069(97)00087-3
9. C. Cui, B.M. Hu, L. Zhao, and S. Liu, Titanium Alloy Production Technology, Market Prospects and Industry Development, *Mater. Des.*, 2011, **32**, p 1684–1691. https://doi.org/10.1016/j.matdes.2010.09.011
10. H. Matsumoto, H. Yoneda, K. Sato, S. Kurosu, E. Maire, D. Fabregue, T.J. Konno, and A. Chiba, Room-Temperature Ductility of Ti-6Al-4V Alloy with α' Martensite Microstructure, *Mater. Sci. Eng. A*, 2011, **528**, p 1512–1520. https://doi.org/10.1016/j.msea.2010.10.070
11. M.J.R. Barboza, E.A.C. Perez, M.M. Medeiros, D.A.P. Reis, M.C.A. Nono, F.P. Neto, and C.R.M. Silva, Creep Behavior of Ti-6Al-4V and a Comparison with Titanium Matrix Composites, *Mater. Sci. Eng. A.*, 2006, **428**, p 319–326. https://doi.org/10.1016/j.msea.2006.05.089
12. Y.K. Kim, S.H. Park, J.H. Yu, B. AlMangour, and K.A. Lee, Improvement in the High-Temperature Creep Properties via Heat Treatment of Ti-6Al-4V Alloy Manufactured by Selective Laser Melting, *Mater. Sci. Eng. A*, 2018, **715**, p 33–40. https://doi.org/10.1016/j.msea.2017.12.085
13. T. Mohandas, D. Banerjee, and V.V. Kutumbarao, Elevated Temperature Properties of Electron Beam Welds of an α + β Titanium Alloy, *Mater. Sci. Eng. A*, 1999, **269**, p 217–224. https://doi.org/10.1016/s0921-5093(99)00172-0
14. R. Filip, K. Kubiak, W. Ziaja, and J. Sieniawski, The Effect of Microstructure on the Mechanical Properties of Two-Phase Titanium Alloys, *J. Mater. Process. Technol*, 2003, **133**, p 84–89. https://doi.org/10.1016/S0924-0136(02)00248-0
15. G. Dai, J. Niu, Y. Guo, Z. Sun, Z. Dan, H. Chang, and L. Zhou, Microstructure Evolution and Grain Refinement Behavior During Hot Deformation of Fe Micro-Alloyed Ti-6Al-4V, *J. Mater. Res. Technol.*, 2021, **15**, p 1881–1895. https://doi.org/10.1016/j.jmrt.2021.09.009
16. J.O. Peters, G. Lütjering, M. Koren, H. Puschnik, and R.R. Boyer, Processing, Microstructure, and Properties of β-CEZ, *Mater. Sci. Eng. A*, 1996, **213**, p 71–80. https://doi.org/10.1016/0921-5093(96)10225-2
17. Z. Sun, S. Guo, and H. Yang, Nucleation and Growth Mechanism of α-Lamellae of Ti Alloy TA15 Cooling from an α + β Phase Field, *Acta Mater.*, 2013, **61**, p 2057–2064. https://doi.org/10.1016/j.actamat.2012.12.025
18. J. Da Costa Teixeira, B. Appolaire, E. Aeby-Gautier, S. Denis, L. Héricher, Modeling of the Phase Transformations in Near-β Titanium Alloys During the Cooling After Forging. Comput. Mater. Sci. 42, 266–280 (2008). https://doi.org/10.1016/j.commatsci.2007.07.056
19. H. Fujii, Continuous Cooling Transformation Characteristics of α + β Titanium Alloys, *Nippon Steel Tech. Rep.*, 1994, **62**, p 74–79.
20. S.L. Semiatin, S.L. Knisley, P.N. Fagin, F. Zhang, and D.R. Barker, Microstructure Evolution During Alpha-Beta Heat Treatment of Ti-6Al-4V, *Metall. Mater. Trans. A*, 2003, **34**, p 2377–2386. https://doi.org/10.1007/s11661-003-0300-0
21. R. Trivedi, The Role of Interfacial Free Energy and Interface Kinetics During the Growth of Precipitate Plates and Needles, *Metall. Trans.*, 1970, **1**, p 921–927.
22. W.P. Bosze and R. Trivedi, On the Kinetics Expression for the Growth of Precipitate Plates, *Metall. Trans.*, 1974, **5**, p 511–512. https://doi.org/10.1007/BF02644122
23. M. Meng, X.G. Fan, H. Yang, L.G. Guo, M. Zhan, and P.F. Gao, Precipitation of Secondary Alpha in Competition with Epitaxial Growth of Primary Alpha in Two-Phase Titanium Alloys, *J. Alloys Compd.*, 2017, **714**, p 294–302. https://doi.org/10.1016/j.jallcom.2017.04.209
24. I. Katzarov, S. Malinov, and W. Sha, Finite Element Modeling of the Morphology of β to α Phase Transformation in Ti-6Al-4V Alloy, *Metall. Mater. Trans. A.*, 2002, **33**, p 1027–1040. https://doi.org/10.1007/s11661-002-0204-4
25. S. Malinov, P. Markovsky, W. Sha, and Z. Guo, Resistivity Study And Computer Modelling of the Isothermal Transformation Kinetics of Ti–6Al–4V and Ti–6Al–2Sn–4Zr–2Mo–0.08Si Alloys, *J. Alloys Compd.*, 2001, **314**, p 181–192. https://doi.org/10.1016/S0925-8388(01)01708-X
26. S. Tanaka, T. Morita, K. Shinoda, Effects of Short-Time Duplex Heat Treatment on Microstructure and Fatigue Strength of Ti-6Al-4V alloy, in: 13th International Conference on Fracture, (2013), pp. 16–21

Accepted Manuscript

27. T. Morita, K. Hatsuoka, T. Iizuka, and K. Kawasaki, Strengthening of Ti-6Al-4V Alloy by Short-Time Duplex Heat Treatment, *Mater. Trans.*, 2005, **46**, p 1681–1686. https://doi.org/10.2320/matertrans.46.1681
28. T. Morita, K. Asakura, and C. Kagaya, Effect of Combination Treatment on Wear Resistance and Strength of Ti-6Al-4V Alloy, *Mater. Sci. Eng. A*, 2014, **618**, p 438–446. https://doi.org/10.1016/j.msea.2014.09.042
29. R. Reda, A. Nofal, and A.H. Hussein, Effect of Single and Duplex Stage Heat Treatment on the Microstructure and Mechanical Properties of Cast Ti-6Al-4v Alloy, *Metallogr. Microstruct. Anal.*, 2013, **2**, p 388–393. https://doi.org/10.1007/s13632-013-0103-7
30. A. Ajiz and J. Gunawarman, Affi, The Effects of Short-Time Solution Treatment and Short-Time Aging on Mechanical Properties of Ti-6Al-4V for Orthopaedic Applications, *Int. J. Adv. Sci. Eng. Inf. Technol.*, 2015, **5**, p 329–334. https://doi.org/10.18517/ijaseit.5.4.556
31. T. Morita, S. Tanaka, and S. Ninomiya, Improvement in Fatigue Strength of Notched Ti-6Al-4V Alloy by Short-Time Heat Treatment, *Mater. Sci. Eng. A*, 2016, **669**, p 127–133. https://doi.org/10.1016/j.msea.2016.05.071
32. B. Sonderegger and E. Kozeschnik, Interfacial Energy of Diffuse Phase Boundaries in the Generalized Broken-Bond Approach, *Metall. Mater. Trans. A*, 2010, **41**, p 3262–3269. https://doi.org/10.1007/s11661-010-0370-8
33. J. Svoboda, F.D. Fischer, P. Fratzl, and E. Kozeschnik, Modelling of Kinetics in Multi-Component Multi-Phase Systems with Spherical Precipitates I: Theory, *Mater. Sci. Eng. A*, 2004, **385**, p 166–174. https://doi.org/10.1016/j.msea.2004.06.018
34. E. Laude, E. Gautier, P. Archambault, and S. Denis, Cinétique de Transformation des Alliages de Titane en Fonction du Traitement Thermomécanique. Etude Expérimentale et Calcul, *Rev. Métallurgie.*, 1996, **93**, p 1067–1078. https://doi.org/10.1051/metal/199693091067
35. G. Gueret, B. Houssin, J. Fries, G. Cizeron, and P. Lacombe, Cinétique de durcissement de l'alliage de titane TA6V6E2. Analyse de l'évolution structurale au cours du revenu, *J. Less Common Met.*, 1974, **38**, p 31–51. https://doi.org/10.1016/0022-5088(74)90201-X
36. S. Bein and J. Béchet, Phase Transformation Kinetics and Mechanisms in Titanium Alloys Ti-6.2.4.6, P-CEZ and Ti-10.2.3, *J. Phys. IV*, 1996, **6**, p 99–108.
37. N. Kherrouba, Étude expérimentale et modélisation des cinétiques de transformation de phase dans un alliage de titane, PhD, Ecole Nationale Polytechnique d'Alger - Université Bretagne Sud, 2017. https://tel.archives-ouvertes.fr/tel-01710754
38. N. Kherrouba, M. Bouabdallah, R. Badji, D. Carron, and M. Amir, Beta to Alpha Transformation Kinetics and Microstructure of Ti-6Al-4V Alloy During Continuous Cooling, *Mater. Chem. Phys.*, 2016, **181**, p 462–469. https://doi.org/10.1016/j.matchemphys.2016.06.082
39. J.W. Elmer, T.A. Palmer, S.S. Babu, and E.D. Specht, In Situ Observations of Lattice Expansion and Transformation Rates of α and β Phases in Ti-6Al-4V, *Mater. Sci. Eng. A*, 2005, **391**, p 104–113. https://doi.org/10.1016/j.msea.2004.08.084
40. J.B. Newkirk, Precipitation from Solid Solution, ASM Int. 104–107 (1959)
41. J. Burke, *The Kinetics of Phase Transformation in Metals*, 1st ed. Pergamon Press, Oxford, 1965
42. D.V. Gadeev and A.G. Illarionov, Determination of Beta-Transus Temperature of Two-Phase Titanium Alloys using differential Scanning Calorimetry, *Solid State Phenom.*, 2018, **284**, p 259–264. https://doi.org/10.4028/www.scientific.net/SSP.284.259
43. J. Da Costa Teixeira, Etude expérimentale et modélisation des évolutions microstructurales au cours des traitements thermiques post forgeage dans l'alliage de titane Ti17, PhD, Institut National Polytechnique de Lorraine (2005). https://hal.archives-ouvertes.fr/tel-00325787
44. J.W. Christian, The Theory of Transformations in Metals and Alloys, 1st ed., Pergamon, (2002)
45. N. Kherrouba, D. Carron, M. Bouabdallah, and R. Badji, Effect of Solution Treatment on the Microstructure, Micromechanical Properties, and Kinetic Parameters of the $\beta \rightarrow \alpha$ Phase Transformation During Continuous Cooling of Ti-6Al-4V Titanium Alloy, *J. Mater. Eng. Perform.*, 2019, **28**, p 6921–6930. https://doi.org/10.1007/s11665-019-04404-5
46. D.A. Porter, K.E. Easterling, and M.Y. Sherif, *Phase Transformations in Metals and Alloys*, 3rd ed. CRC Press Taylor and Francis, Boca Raton, 2009
47. M. Tiryakioğlu, G. Ökten, and D. Hudak, Statistics for Estimating the Population Average of a Lifshitz-Slyozov- Wagner (LSW) Distribution, *J. Mater. Sci.*, 2009, **44**, p 5754–5759. https://doi.org/10.1007/s10853-009-3806-z
48. S.L. Semiatin, B.C. Kirby, and G.A. Salishchev, Coarsening Behavior of an Alpha-Beta Titanium Alloy, *Metall. Mater. Trans. A.*, 2004, **35**, p 2809–2819.
49. J. Xu, W. Zeng, Z. Jia, X. Sun, and Y. Zhao, Coarsening Kinetics and Morphological Evolution in a Two-Phase Titanium Alloy During Heat Treatment, *J. Mater. Eng. Perform.*, 2016, **25**, p 734–743. https://doi.org/10.1007/s11665-016-1951-5
50. N. Stefansson and S.L. Semiatin, Mechanisms of Globularization of Ti-6Al-4V During Static Heat Treatment, *Metall. Mater. Trans. A.*, 2003, **34**, p 691–698.

Accepted Manuscript